

# Soft Wearable Systems for Colorimetric and Electrochemical Analysis of Biofluids

Roozbeh Ghaffari,\* Jungil Choi, Milan S. Raj, Shulin Chen, Stephen P. Lee, Jonathan T. Reeder, Alexander J. Aranyosi, Adam Leech, Weihua Li, Stephanie Schon, Jeffrey B. Model, and John A. Rogers\*

Wearable monitoring systems provide valuable insights about the state of wellness, performance, and progression of diseases. Although conventional wearable systems have been effective in measuring a few key biophysical markers, they offer limited insights into biochemical activity and are otherwise cumbersome in ambulatory modes of use, relying on wired connections, mechanical straps, and bulky electronics. Recent advances in skin-interfaced microfluidics, stretchable/flexible electronics, and mechanics have created new wearable systems with capabilities in real-time, noninvasive analysis of sweat biochemistry in combination with biophysical metrics. Here, the latest technologies in multifunctional sweat sensing systems are presented with a focus on novel microfluidic designs, fully-integrated wireless electrochemical sensors, and hybrid biochemical/biophysical sensing capabilities, creating real-time physiological insights.

biochemical health monitoring capabilities with implications for chronic care management, performance tracking, and triage in military settings.<sup>[1]</sup> Despite the popularity of existing wearable technologies, their utility in these remote settings remains restricted because of their bulky packaging and rigid/boxy designs, which in turn, give rise to poor signal quality, discomfort, and poor compliance.<sup>[2]</sup> Moreover, biochemical sensing systems are limited to measuring a few important biometrics within the confines of controlled laboratory settings. As such, multiparameter monitoring of biophysical and biochemical signals in the field requires having the subject wear multiple disparate systems at once

with trained technician and field support. Not only is this mode of operation physically uncomfortable, it can also be cost-prohibitive.

Recent advances in flexible hybrid electronics and microfluidics have led to new classes of physiological and biochemical sensors that noninvasively capture and interrogate biofluids, such as sweat, tears, and saliva.<sup>[3]</sup> Sweat sensing, in particular, offers unique routes for real-time analysis of ambulatory human metabolic activity, underpinning the physiological state.<sup>[4]</sup> The ability to couple soft microfluidic substrates with skin-like electronic modules has led to entirely new classes of wearable biochemical sensing systems with onboard memory, power, and wireless connectivity. The integration of biophysical and biochemical sensing with wireless connectivity to smartphones and data acquisition modules is of keen interest to clinicians, researchers, athletes, and consumers.

This review presents the current state of the art in wearable colorimetric and electrochemical sweat sensing technologies and highlights the convergence of these sensing modalities with epidermal electronics and physiological monitoring. Sections 2–4 provide summaries of passive microfluidic-based systems, electrochemical sensing systems, and recent demonstrations of hybrid systems that combine both biophysical and biochemical sensing. The review ends with a look at future directions and opportunities for biochemical sensing and the path to fully-integrated multimodal physio-biochemical wearable systems.

## 1. Introduction

Wearable biosensing systems that interface with the human skin provide powerful biophysical, kinematic, and

Prof. R. Ghaffari, M. S. Raj, S. Chen, S. P. Lee, Dr. A. J. Aranyosi, A. Leech, W. Li, J. B. Model  
Epicore Biosystems, Inc.  
Cambridge, MA 02139, USA  
E-mail: rooz@epicorebiosystems.com

Prof. R. Ghaffari, M. S. Raj, S. Chen, S. P. Lee, Dr. J. T. Reeder, Dr. A. J. Aranyosi, S. Schon, J. B. Model, Prof. J. A. Rogers  
Center for Bio-Integrated Electronics  
Northwestern University  
Evanston, IL 60208, USA  
E-mail: jrogers@northwestern.edu

Prof. R. Ghaffari, Prof. J. A. Rogers  
Department of Biomedical Engineering  
Northwestern University  
Evanston, IL 60208, USA

Prof. J. Choi  
School of Mechanical Engineering  
Kookmin University  
Seoul 02707, Republic of Korea

Prof. J. A. Rogers  
Department of Materials Science and Engineering  
Northwestern University  
Evanston, IL 60208, USA

 The ORCID identification number(s) for the author(s) of this article can be found under <https://doi.org/10.1002/adfm.201907269>.

DOI: 10.1002/adfm.201907269

## 2. Epidermal Microfluidics with Colorimetric-Based Sensing

Eccrine sweat excreted from skin pores contains a rich blend of electrolytes, metabolites, proteins, hormones, and exogenous agents.<sup>[5]</sup> These sweat constituents vary regionally across anatomical locations,<sup>[6]</sup> are modulated by diet, mental stress, physiological state, and environmental factors (e.g., humidity, ambient temperature), and could vary diurnally.<sup>[7]</sup> Conventional gravimetric and lab-based tools have been widely used to study sweat biocomposition and dynamics, providing foundational knowledge about the effects of heat stress and proper hydration based on analysis conducted within controlled laboratory settings. Recent advances in wearable biosensor technologies have begun unlocking new insights about sweat biomarkers and their correlation with physiology, hydration, and performance in more remote environments untethered from expensive laboratory equipment and bulky benchtop analyzers.<sup>[3c,4b,8]</sup> Soft, wearable microfluidics systems constructed from soft elastomeric materials (e.g., silicones) provide a unique platform for collection, storage, and on-board analysis of sweat excreted directly from skin pores.<sup>[9]</sup> These devices conformally integrate with the skin as a result of their low bending stiffness, soft material properties, and a patterned hypoallergenic adhesive layer. Sweat glands create hydraulic pressure from differences of osmolality between sweat and plasma which actively induces sweat flow into the epifluidic device.<sup>[5b]</sup> A water-tight adhesive seal between the skin and the device directs sweat flow into the networks of microchannels and microreservoirs which provide collection and storage capabilities.<sup>[10]</sup> The addition of colorimetric assays in the form of dry reagents to reaction chambers built within the device allow for colorimetric analysis of sweat. Examples of well-established colorimetric assays compatible with epifluidic devices include those which detect electrolytes, metabolites, and proteins.<sup>[9,11]</sup> The devices collect sweat and analyze multiple physiological parameters, including local sweat loss/rate and time-variant biocomposition without requiring battery-powered actuators or active valves.<sup>[10,12]</sup>

The ability to collect sweat underwater rises from the construction of high-water barrier materials and geometrical considerations for the device outlet, preventing external fluid from entering the microchannel space.<sup>[13]</sup> The device is constructed from poly(styrene-isoprene-styrene) (SIS) which has exceptionally high-water barrier properties. The sweat inlet is sealed to the skin in an air-tight and water-tight fashion, allowing sweat to proceed into the device while simultaneously preventing contamination via environmental fluids. Environmental water is prevented from entering the outlet of the device due to the hydrophobicity of the SIS and the small diameter of the outlet aperture (**Figure 1a**). Integrating flexible hybrid electronic modules embedded in this fluidic device offers additional capabilities, including near field communication (NFC) and skin temperature measurements. By virtue of its soft material properties (0.83 MPa), these SIS fluidic devices can support bending, flexure, and multidimensional strains exceeding 400% (**Figure 1b,c**). Their unique tapered geometries create a robust water-proof seal on the skin which enables contamination-free capture of sweat in swimming pool and open ocean environments (**Figure 1d**). Integrated colorimetric bioassays



**Roozbeh Ghaffari** obtained his B.S. and M.E. degrees in electrical engineering from the Massachusetts Institute of Technology in 2001 and 2003. He received his Ph.D. degree in biomedical engineering from the Harvard Medical School–MIT Program in Health Sciences and Technology in 2008. He joined the Center for Bio-

Integrated Electronics at Northwestern University in May 2017, where he is currently a research associate professor in the Department of Biomedical Engineering and serves as a Director of Translational Research. His research interests lie at the intersection of soft microfluidics, bioelectronics, biosensors, and precision medicine.



**Jungil Choi** obtained his Ph.D. in electrical engineering in 2015, and S.M. and B.S. degrees in mechanical and aerospace engineering in 2010 and 2008 at Seoul National University. He is currently an assistant professor in the department of mechanical engineering at Kookmin University. He completed his postdoctoral

research program in the Rogers group at the Center for Bio-Integrated Electronics at Northwestern University. His research focus is in the application of microfluidics technology in biomedical applications, including wearable sweat analytics systems, smart farm systems, and imaging-based drug testing.



**John A. Rogers** obtained B.A. and B.S. degrees in chemistry and in physics from the University of Texas Austin, in 1989. From MIT, he received S.M. degrees in physics and in chemistry in 1992 and his Ph.D. degree in physical chemistry in 1995. In 2016, he joined Northwestern University as the Louis Simpson and

Kimberly Querrey Professor of Materials Science and Engineering, Biomedical Engineering, and Medicine, with affiliate appointments in Mechanical Engineering, Electrical and Computer Engineering, and Chemistry, where he is also Executive Director of the Center for Bio-Integrated Electronics.

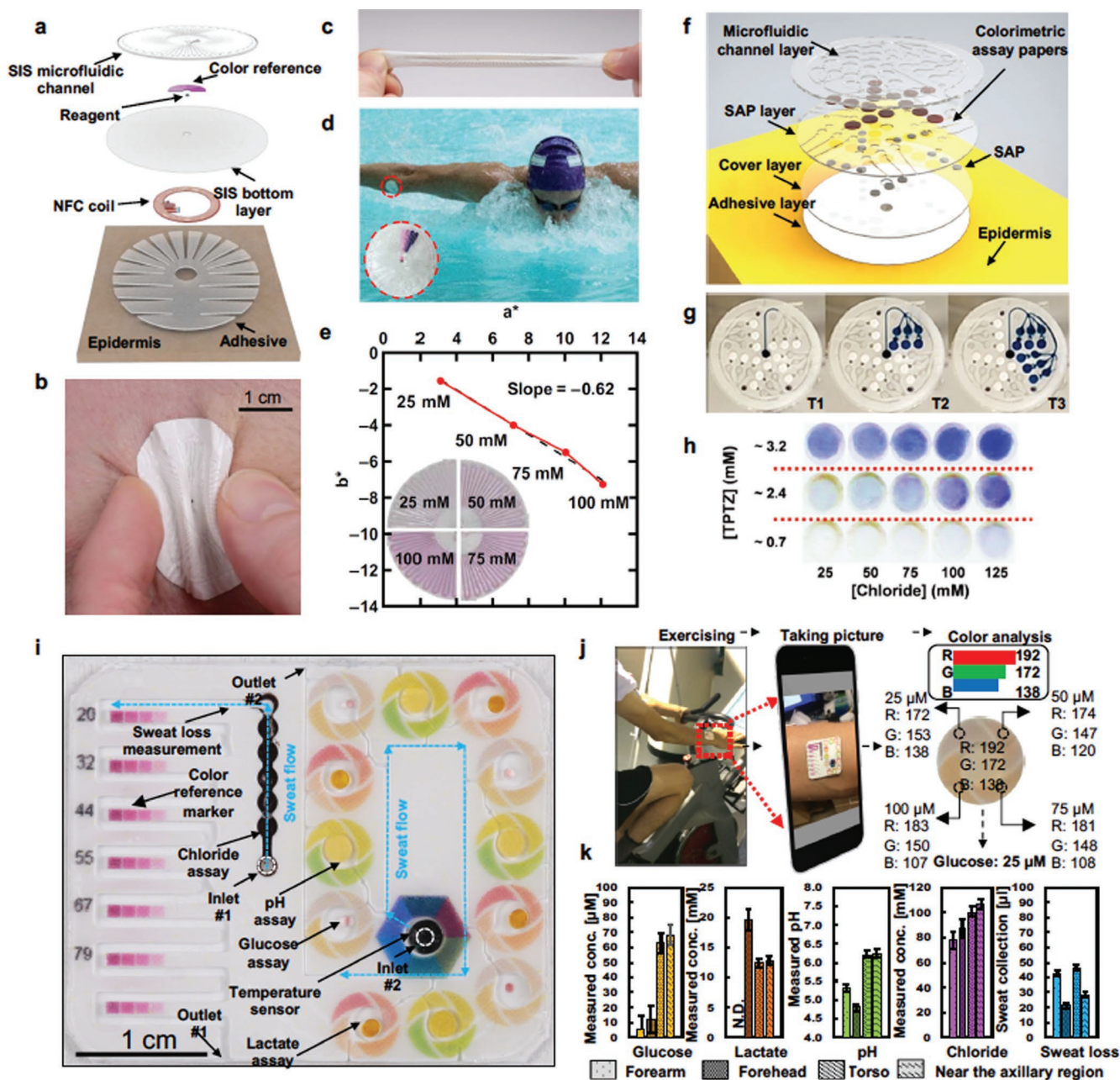


**Figure 1.** Latest biochemical monitoring wearable systems (microfluidic and colorimetric designs). a) Schematic illustration showing an exploded view of the sublayers of waterproof SIS microfluidic/electronic device. b) Optical image of SIS device with tapered edges on the skin under compression. c) Optical image of device being stretched by 400%. d) Optical image of device being worn on subject during swimming exercise. Inset: magnified image of the skin-mounted device filling with sweat. e) The  $a^*$  and  $b^*$  color values associated with reference chloride solutions after reacting with silver-chloranilate. Inset: Photographs of poly(styrene-isoprene-styrene) devices showing colorimetric responses corresponding to  $25 \times 10^{-3}$ ,  $50 \times 10^{-3}$ ,  $75 \times 10^{-3}$ , and  $100 \times 10^{-3}$  M chloride concentrations. a–e) Reproduced with permission.<sup>[13]</sup> Copyright 2019, American Association for the Advancement of Science. f) Exploded schematic illustration of chrono-sampling epidermal microfluidic device. g) Optical images showing chrono-sampling of artificial sweat at different time snapshots (T1, T2, T3). h) Color development of assays at varying levels of TPTZ ( $0.7 \times 10^{-3}$ ,  $2.4 \times 10^{-3}$ ,  $3.2 \times 10^{-3}$  M) and their corresponding colorimetric response generated by different chloride concentrations ( $25 \times 10^{-3}$ ,  $50 \times 10^{-3}$ ,  $75 \times 10^{-3}$ ,  $100 \times 10^{-3}$ ,  $125 \times 10^{-3}$  M). Reproduced with permission.<sup>[15]</sup> Copyright 2018, Wiley-VCH. i) Magnified image of a soft, flexible, multifunctional microfluidic device for colorimetric analysis of sweat biomarkers (pH, glucose, lactate, chloride, sweat flow, and temperature). j) Sequence of images showing microfluidic device worn on the inner forearm of subject during exercise (left panel), image snapshot taken with smartphone camera (middle panel), and magnified view of glucose assay (right panel). k) Representative field test data showing regional variations of sweat concentration (glucose, lactate, pH, chloride, and sweat loss) from different body positions; forearm, forehead, chest, and below the armpit from subject N.D. represents data not collected due to insufficient sweat generation. Reproduced with permission.<sup>[11a]</sup> Copyright 2019, American Chemical Society.

(e.g., chloride) preinjected in the device mix with sweat as it propagates through, enabling real-time measurement of sweat rate, sweat loss, and chloride concentration via optical readout (Figure 1e). Sweat loss is measured either by the naked eye or by capturing an image of the device. Observation of the number of filled microchannel turns and the known volume of each turn allows calculation of the sweat volume. Multiple images taken in known time sequence enable calculation of sweat rate. For colorimetric assay measurement, color analysis is performed using the LAB color space with “L,” “a,” and “b” representing the three principal axes. Color is expressed as:  $L^*$  for the lightness from black (0) to white (100),  $a^*$  from green (–) to red (+), and  $b^*$  from blue (–) to yellow (+). The reference data shown in Figure 1e forms a characteristic vector in  $a^*b^*$  space, illustrating the change in sweat color after reacting with silver-based assay.  $A^*$  and  $b^*$  color values are then compared to the reference vector for calculating the chloride concentration. The collection diameter of  $\approx 6$  mm on the skin and a sweat collection reservoir of 60  $\mu\text{L}$  support a broad range of sweat rate measurements ranging from 3 to 34  $\mu\text{L h}^{-1}$ . Local sweat and electrolyte measurements are then collectively correlated to whole body fluid/electrolyte loss of sweat and can be used to determine rehydration strategies after land-based and aquatic exercise activities.<sup>[14]</sup> The addition of passive electronic components including those for power harvesting, data communication, and sensors provides additional functionality for wireless collection of biophysical events. In this example, an on-board temperature sensor enables skin temperature to be wirelessly recorded via nearby coupling between a flexible NFC device embedded in the epifluidic device and an NFC-enabled smartphone.

The ability to dynamically handle and redirect sweat flow in microfluidic devices is a key feature required for advanced functionalities, such as time sequential sweat characterization. Wearable microfluidic valve designs and actuating structures have recently been developed, utilizing superabsorbent polymers (SAP) of sodium polyacrylate and unique microchannel geometries ( $\approx 2.4$  mm: the diameter of reservoirs). These materials and micrometer-scale channel structures control the flow of sweat ( $\approx 40$   $\mu\text{L}$ ) through the microfluidic devices in a highly tunable time sequential manner<sup>[15]</sup> (Figure 1f). Representative devices are multilayered, consisting of SAP and colorimetric assays (e.g., chloride) integrated within the fluidics channels (Figure 1g). Sweat ingress into the SAP material induces volumetric swelling which physically blocks the inlet of the reservoir and induces sweat to proceed to the subsequent reservoir. A preloaded colorimetric assay that exploits competitive chelation between  $\text{Fe}^{2+}$  and  $\text{Hg}^{2+}$  using 2,4,6-tris(2-pyridyl)-s-triazine (TPTZ) and color changes corresponding to chloride levels ( $25\text{--}125 \times 10^{-3}$  M) (Figure 1h). As the network of microchannels and wells fill sequentially, the wearer is able to track changes in biomarker concentration as a function of time and activity type.

Integration of the materials, mechanics, and microfluidic design strategies described above enable multifunctional microfluidic devices which measure local sweat dynamics and multiple time-dependent biomarker concentrations concurrently, including chloride, pH, glucose and lactate, and skin/sweat temperature.<sup>[11a]</sup> A representative device, shown in Figure 1i, consists of a network of microfluidic channels for quantifying sweat loss, an array of colorimetric assays, and a thermochromic

liquid crystal-based temperature sensor located within the microfluidic channel. A 600  $\mu\text{m}$  deep assay reservoir allows optical absorption and a measurable color change, resulting in increased accuracy of imaging processing for chloride ( $10\text{--}125 \times 10^{-3}$  M), pH (4.5–7), glucose ( $10\text{--}125 \times 10^{-6}$  M), and lactate ( $5\text{--}20 \times 10^{-3}$  M). Capillary burst valves with engineered burst pressures enable filling of a set of chambers in a defined sequence, and multitime-point analysis of multiple sweat biomarkers in a single device. Color reference markers on the top-most layer of the device are matched with the color changes in the microfluidics with a smartphone camera, which is used to determine the bioassay concentrations and to correct for various ambient lighting conditions (Figure 1j). This colorimetric analysis technique has signal uncertainties corresponding to  $\approx 1 \times 10^{-3}$  M for chloride,  $\approx 3 \times 10^{-6}$  M for glucose,  $\approx 0.1$  for pH, and  $\approx 2 \times 10^{-3}$  M for lactate. Field testing results taken from multimodal microfluidic devices attached to multiple anatomical locations (e.g., forearm, forehead, chest, and under arm) during exercise demonstrate the potential for mapping real-time changes in sweat biomarkers across a diverse range of environments, not possible using standard lab-based measurement tools (Figure 1k).

### 3. Epidermal Electrochemical Sensing Systems

Colorimetric-based epidermal microfluidic systems provide insights about sweat concentrations and dynamics at discrete points in time; but this class of biochemical sensor does not provide continuous tracking. Electrochemical sensors constitute a powerful measurement tool for measuring electrolytes, metabolites, and protein targets.<sup>[16]</sup> Biochemical data captured and transmitted, in digital formats, by wireless wearable electrochemical sensors establish high resolution tracking of metabolic activity and physiological status in remote environments.<sup>[17]</sup> Although this capability set is critical for continuous monitoring, there are important tradeoffs in power consumption and device footprint that must be considered.<sup>[17a]</sup>

To achieve wide scale adoption of electrochemical sweat sensing technology requires rigorous testing and clinical validation studies benchmarking sweat concentrations and latency in time compared to blood-based analysis. A recent electrochemical study has established the correlation between sweat ethanol and blood ethanol levels via a sweat biosensing device with an integrated sweat stimulation system.<sup>[18]</sup> The device stimulates sweat via iontophoresis of carbachol through electrical stimulation ( $\approx 0.28$  mA  $\text{cm}^{-2}$ ), which generates sweat flow rates of up to 320 nL  $\text{min}^{-1}$  from the targeted skin region ( $\approx 0.8$   $\text{cm}^2$ ) (Figure 2a,b). The amperometric electrochemical sensor measures the concentration of ethanol in sweat by measuring the electrical current generated by the release of electrons during the reduction of ethanol to hydrogen peroxide by alcohol oxidase. Sweat ethanol concentrations peak prior to dissipating over time and were shown to correlate with blood alcohol concentrations with a delay of  $\approx 7$  min (Figure 2b).

Physical exercise is an effective way to induce sweat excretion for biochemical sensing studies; but is often infeasible for vulnerable populations (e.g., infant and elderly patients). Delivery of sweat-stimulating pharmacologic agents, such as pilocarpine,

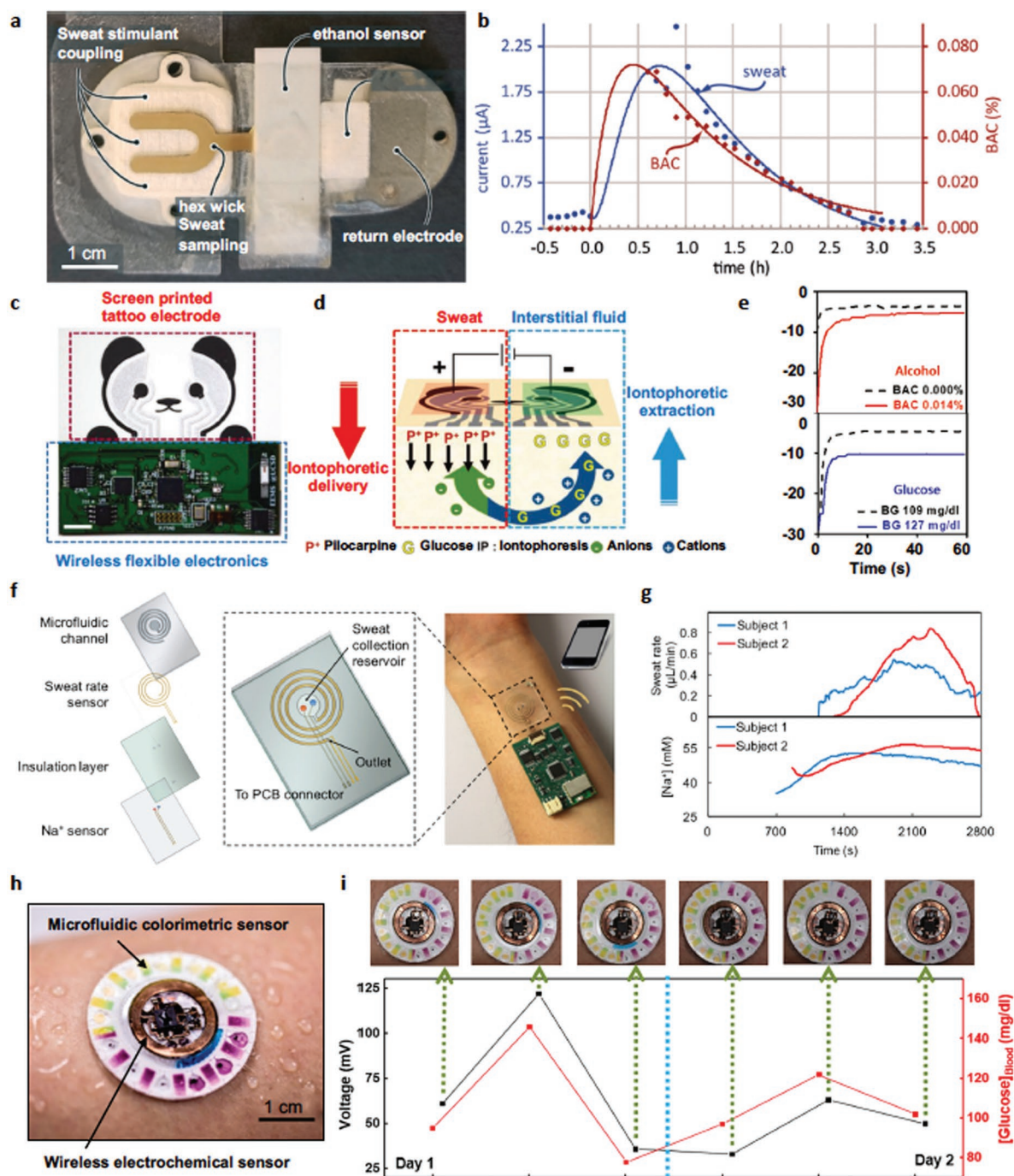


**Figure 2.** Latest biochemical monitoring wearable systems (electro-fluidic, electrochemical designs). a) Optical image of sweat sensor device with integrated sweat stimulation and ethanol sensing capabilities. b) Representative in situ data and pharmacokinetic model fits the subject data. Reproduced with permission.<sup>[18]</sup> Copyright 2018, The Royal Society of Chemistry. c) Optical image of screen-printed sweat sensor with integrated flexible printed circuit board. Scale bar: 7 mm. d) Schematic drawing illustrating sweat and interstitial fluid extraction using iontophoretic delivery of pilocarpine for inducing sweat and measuring glucose concentrations. e) Representative data of glucose/alcohol biosensor showing amperometric response as a function of time under experimental condition for human subject with consumption of meal and alcohol beverage. Reproduced with permission.<sup>[19]</sup> Copyright 2018, Wiley-VCH. f) Schematic drawings showing exploded view of a wearable sweat sensing patch composed of a microfluidic sweat sensor, Au electrodes for sweat rate sensing, parylene-C insulation layer, Na<sup>+</sup> sensing electrodes, and a Bluetooth wireless communication module. g) Simultaneous on-body measurements of sweat rate and [Na<sup>+</sup>] using the sweat sensing patch during cycling field testing. Reproduced with permission.<sup>[21]</sup> Copyright 2019, American Chemical Society. h) Optical image of hybrid colorimetric, electrochemical battery-free system on the skin. i) Optical images showing the filling at different times during sweating over a 2-d period (top). (Bottom) Correlation of data acquired for sweat glucose sweat sensor compared to blood glucose measured at same points in time over a 2 d period. Reproduced with permission.<sup>[22]</sup> Copyright 2019, American Association for the Advancement of Science.

to the skin generate local sweat release without requiring exercise. Recent development of wearable devices with onboard iontophoretic delivery and extraction functionality has enabled parallel extraction of sweat and interstitial fluid (ISF) from the skin. Sweat-inducing pilocarpine was delivered using an applied current (0.8 mA) into the dermis at the anode to induce sweat release, whereas at the cathode compartment, reverse iontophoretic system extracts ISF for analysis. As a result, the device was able to measure both glucose and ethanol levels in ISF and sweat simultaneously from neighboring regions of the skin (Figure 2c–e).<sup>[19]</sup> The enzymes (glucose oxidase for glucose and alcohol oxidase for alcohol) are immobilized by chitosan with Prussian blue (PB) transducer to form the electrodes. The amperometric reaction at the anode tracks alcohol in sweat and detects glucose in ISF at the cathode. The reduction of hydrogen peroxide resulting from this enzymatic reaction produces an amperometric signal. On-body field testing highlighted differences in ethanol and glucose levels in sweat, ISF, and blood. Food and alcohol consumption gives rise to similar trends in glucose and ethanol concentrations in sweat and ISF biofluids (Figure 2e).

Continuous measurements of sweat rate (and thus sweat volume)<sup>[20]</sup> and electrolyte levels<sup>[21]</sup> are enabled via the placement of parallel electrodes which run longitudinally along a microfluidic channel (Figure 2f). The impedance between the electrodes is dictated by both the volume of sweat captured in the microfluidic channel as well as electrolyte concentrations ( $H^+$ ,  $Na^+$ ,  $K^+$ , and  $Cl^-$ ) and enables simultaneous measurements of both.<sup>[21]</sup>  $Na^+$  sensing electrodes located at the inlet of the microfluidic channel composed of ion-selective electrodes and a polyvinyl butyral-coated reference electrode measures  $Na^+$  concentrations. A printed circuit board with a Bluetooth wireless communication module is connected to the electrochemical sensors, facilitating wireless transfer of data from the wearable device to a smartphone (Figure 2f, right panel). Field trials with this electrochemical sensing system on subjects demonstrate the ability to simultaneously measure sweat rate (with  $\approx 90\%$  accuracy), and sodium levels within the physiological range and similar to those measured using conventional methods, such as the Macroduct system (Figure 2g).

Another microfluidic device design combines the advantages of microfluidics, colorimetric sensing, near field communication, and electrochemical sensing in a single device. This hybrid electrochemical-colorimetric system provides multimodal analysis of sweat rate, pH, sweat chloride using a colorimetric approach and glucose and lactate sensing using an NFC-enabled amperometric sensing approach (Figure 2h).<sup>[22]</sup> Electrochemical sensors embedded in the microfluidic channel detect sweat glucose and lactate concentrations from the inner volar forearm. For glucose concentration analysis, the glucose oxidase enzyme is dispersed in the Nafion, causing oxidation of glucose (i.e., release of electrons) and generating a voltage signal that is proportional to the concentration of glucose. The NFC module in the device allows for energy harvesting and data transfer from the electrochemical sensor to a smartphone in close proximity to the device ( $\approx 18$  cm). Human trials conducted over a 2 d period show the relationship between sweat and blood for glucose levels (Figure 2i), thereby highlighting the potential for quantitative monitoring of sweat metabolites in remote settings and in real-time.

## 4. Hybrid Physiological and Biochemical Sensing Systems

Skin-interfaced biochemical systems provide insight about metabolic activity underpinning both the performance and physiology of the wearer. To develop a full understanding of health and performance status requires continuous tracking of biochemical monitoring in combination with environmental and biophysical monitoring.<sup>[23]</sup> Recent advances in biosensing systems, which track sweat biochemical data (e.g., sodium-chloride,<sup>[24]</sup> lactate,<sup>[25]</sup> glucose,<sup>[26]</sup> cortisol levels<sup>[27]</sup>) in conjunction with biophysical signals (e.g., body movements,<sup>[28]</sup> heart rate,<sup>[29]</sup> blood pressure,<sup>[30]</sup> electrocardiogram,<sup>[31]</sup> body temperature<sup>[32]</sup>) are poised to enable real-time ambulatory mapping of human physiology and metabolic activity in ways that were not possible until now. Recent studies have demonstrated multifunctional devices that measure sweat glucose levels as well as heart rate (HR), blood oxygen saturation level ( $SpO_2$ ), and physical activity.<sup>[33]</sup> A representative example of such a system consists of a sweat strip with integrated amperometric sensors to analyze glucose levels in tiny droplets of sweat. The smart band also has a biophysical sensing module, consisting of a multi-axis accelerometer and a light emitting diode coupled to a photodetector for optical measurements of pulse waveforms, HR and  $SpO_2$  signals (Figure 3a). Once sweat is captured in the disposable glucose sensor strip, the strip is then inserted into the smart band for analysis (Figure 3b). The ribbon-like electrochemical glucose sensor uses water-proof overlay film that prevents evaporation of sweat and promotes sweat migration into a microfluidic channel inside the smart wrist band. Measurements of sweat glucose and activity levels are then used to predict caloric expenditure pre- and postexercise (Figure 3b,c).

Another electrochemical/biophysical sensing approach exploits flexible ion-sensitive field-effect transistor sensors to measure sweat pH and collocated flexible printed resistive temperature sensor to measure skin temperature<sup>[34]</sup> (Figure 3d). pH levels in sweat and skin temperature were concurrently tracking, as a means to monitor over-heating exposure during exercise. The pH sensor operates by measuring the concentration of hydrogen ions corresponding to positive potential difference, corresponding to the pH of sweat. An  $Al_2O_3$  layer serves as the ion-sensitive membrane (Figure 3e,f). Hydrogen ions interact with the  $Al_2O_3$  layer changing the top-gate bias of the InGaZnO transistor, which in turn, changes threshold voltages according to the pH value. Initial field testing shows pH values of sweat are stable at  $pH \approx 4.0$ , and skin temperature estimates in the  $30.0\text{--}31.7$  °C range, consistent with commercially available temperature and pH sensors (Figure 3g).

Fully-integrated hybrid systems with integrated physiological monitoring, microfluidics, on-board memory, and a rechargeable battery offer a full suite of biochemical (using electrochemical or colorimetric sensors) and biophysical sensing in a single unified device (Figure 3h). The soft, microfluidic base layer serves as the interface with the skin and provides sweat capture and analysis, while providing a substrate for mechanical coupling to a multiuse/rechargeable flexible hybrid electronic module that supports photoplethysmography, movement

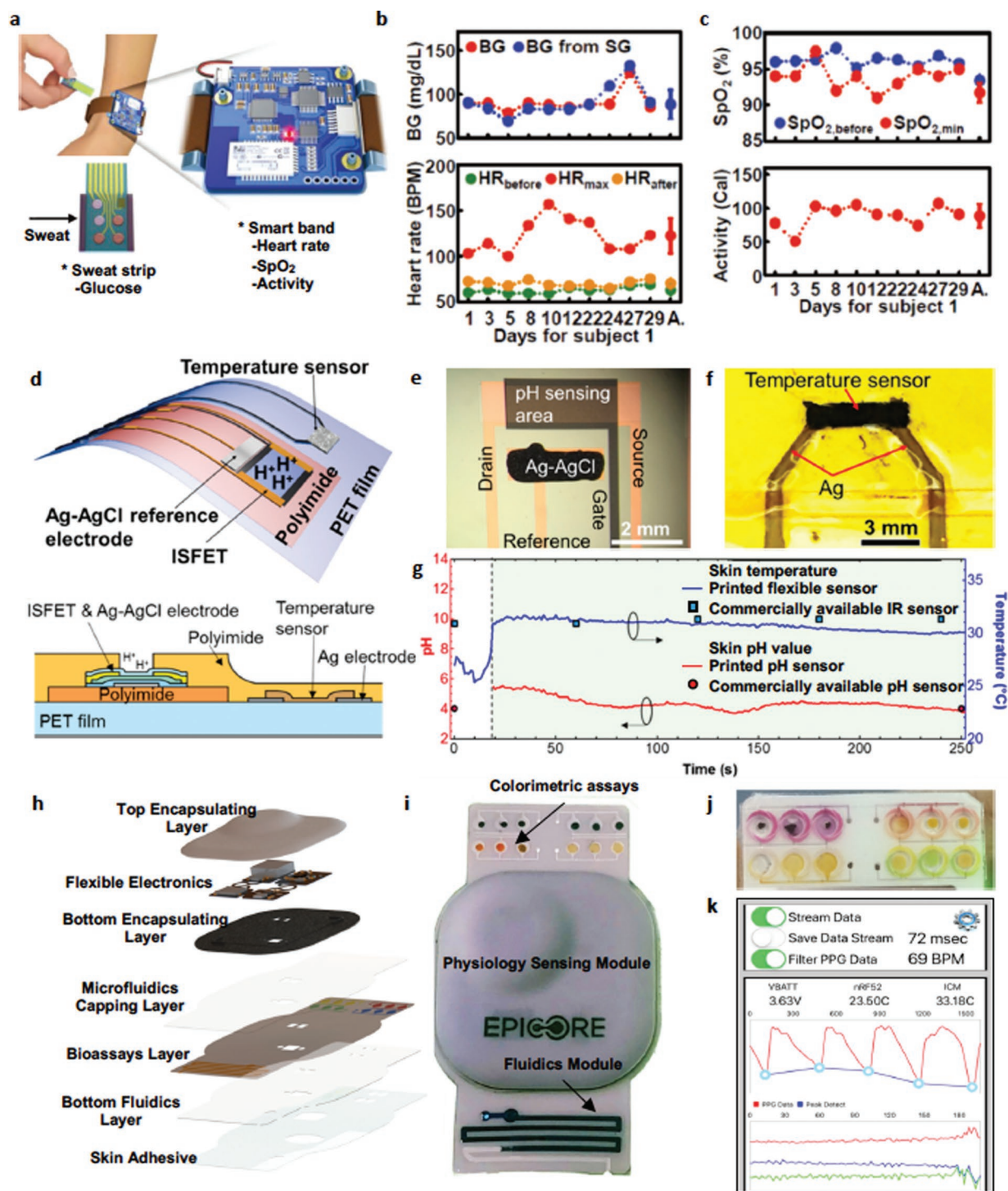


**Figure 3.** Latest hybrid biochem/physio monitoring systems (wrist worn + skin designs). a) Conceptual illustration of a multifunctional wrist-worn wearable system that has a disposable sweat-analysis strip for glucose measurement and a wearable smart band for monitoring heart rate, blood oxygen saturation level (SpO<sub>2</sub>), and physical activity. b,c) Electrochemical sensing data showing glucose in sweat and compared to blood glucose as a function of time, along with simultaneous measurements of heart rate, SpO<sub>2</sub>, and activity. Reproduced with permission.<sup>[33]</sup> Copyright 2018, Wiley-VCH. d) Schematic drawing of wearable device with integrated flexible pH and temperature sensors (top). Cross-sectional diagram of the device (bottom). e) Optical micrograph of the ion-sensitive field-effect transistor pH sensor, gate, source, and drain. f) Optical image of temperature sensor and silver traces. g) Representative data showing pH and skin temperature as a function of time acquired by the device. Reproduced with permission.<sup>[34]</sup> Copyright 2017, American Chemical Society. h) Exploded view of epidermal microfluidic substrate with modular biophysical sensing module. i) Photograph of the integrated device with colorimetric assays, fluidics, and physiological sensors. j) Optical image of multiplexed colorimetric assays for chloride, pH, lactate, and glucose concentrations. k) Snapshot of multimodal pulse waveform and body motion data using the biophysical sensing module.

tracking, and skin temperature sensing (Figure 3i). Sweat biochemistry is analyzed via colorimetric readout using a smartphone camera and image processing software (Figure 3j). The multifunctional colorimetric assays could measure a range of bioanalytes, including sweat chloride ( $10\text{--}100 \times 10^{-3}$  M), sweat glucose ( $25\text{--}100 \times 10^{-6}$  M), pH (4.5–6.5), and sweat lactate ( $5\text{--}20 \times 10^{-3}$  M) (Figure 3j). The flexible electronics module provides continuous streams of biophysical data, which can be fused with the biochemical insights. The electronics include a Bluetooth 5 wireless radio for communication, a flash memory module (128 MB), 3-axis accelerometer and gyroscope unit, an optical sensor, a skin temperature sensor, and a rechargeable thin film battery (12 mAh). The accelerometer and gyroscope unit have an adjustable sampling rate (50–500 Hz) and 16-bit resolution, which is tuned for capturing fine muscle movements as well as gross linear and angular motions of the body (e.g., torso, limb movements). The optical sensor consists of a green light emitting diode (580 nm) and photodetector with an adjustable sampling rate (100 Hz–1 kHz), which is well suited for measuring continuous pulse waveforms and heart rate from different anatomical locations. These multifunctional datasets are stored locally in flash memory or could be streamed via Bluetooth (in real-time) to a smartphone for display and analysis (Figure 3k). Such an electronic-enabled biophysical and biochemical sensing system has soft mechanics and waterproof encapsulation to help withstand various environmental conditions, including temperature fluctuations, moisture exposure, and stress/strain cycles.

## 5. High Throughput Manufacturing and Commercialization

The transition of these prototype wearable systems from feasibility to product development and commercialization requires assessment of regulatory, clinical, and quality strategies, as well as evaluation of manufacturing supply chains needed for scale up beyond university fabrication labs. Recent research in manufacturing methodologies have shown that electrochemical sensors and microfluidics are compatible with low cost, high volume process flows.<sup>[9,35]</sup> A few recent examples of wearable systems, like the FDA-cleared BioStamp system,<sup>[36]</sup> have established full-scale manufacturing, quality, and commercial deployment of skin-interfaced flexible hybrid electronics manufacturing.

Skin-interfaced microfluidic systems are similarly entering the commercialization phase with low-cost (<\$0.50 per unit) and high volume (>10-million units) roll-to-roll manufacturing methods. Key representative examples that highlight this manufacturing scale up, in progress, include a wearable sweat sensing device called the G<sup>2</sup> Sweat Patch<sup>[37]</sup> and the Skin Track pH sweat sensor used for tracking skin/sweat pH balance.<sup>[38]</sup> These novel skin-interfaced microfluidic products for personalized performance and skin-care management are being commercialized by The Gatorade Company, L'Oreal, and Epicore Biosystems. As products continue to mature in this nascent field, the convergence of flexible hybrid electronics and roll-to-roll manufacturing processes will also continue to develop, fostering the integration of biophysical and biochemical sensor modules in fully-integrated wearable systems. These

demonstrations of novel manufacturing methods and examples of commercially deployed wearable microfluidics and bio-sensing systems highlight the potential for broad scale adoption in sports, consumer wellness, and healthcare industries.

## 6. Conclusions

Recent advances in flexible/stretchable electronics, skin-interfaced microfluidics, and soft packaging technologies have created new classes of wearable microfluidics, electrochemical sensors, and hybrid biophysical-biochemical systems. Demonstrations of these novel wearable systems in measuring sweat biomarker and biophysical signals in both controlled and remote field settings show promise for clinical validation and broad scale deployment in health, wellness, and sports applications. Further multidisciplinary research and development in the areas of bio-assay stability in uncontrolled environments, mechanical ruggedness, biosensor development, and understanding of compensatory sweating mechanisms will help to expand the suite of biomarkers and improve accuracy, leading to fully-integrated wearable biosensors that create real-time insights based on both biophysical and the biochemical underpinnings of the human body.

## Acknowledgements

R.G. and J.C. contributed equally to this work. This research was supported by the Northwestern University Center for Bio-Integrated Electronics and the Simpson Querrey Institute for BioNanotechnology. This work was supported by the National Research Foundation of Korea (NRF) grant funded by the Korea government. (MSIT) (NRF-2019R1A2C1084419).

## Conflict of Interest

R.G., M.S.R., S.P.L., A.J.A., J.B.M., and J.A.R. are co-founders of Epicore Biosystems, which is pursuing commercialization of wearable microfluidic devices. A.L., W.L., and S.C. are employees of Epicore Biosystems. The remaining authors are not aware of any affiliations, memberships, funding, or financial holdings that might be perceived as affecting the objectivity of this review.

## Keywords

bioassays, bioelectronics, electrochemistry, microfluidics, personalized medicine

Received: September 3, 2019

Revised: October 6, 2019

Published online: December 1, 2019

- [1] a) T. R. Ray, J. Choi, A. J. Bandodkar, S. Krishnan, P. Gutruf, L. Tian, R. Ghaffari, J. A. Rogers, *Chem. Rev.* **2019**, *119*, 5461; b) K. Takei, W. Gao, C. Wang, A. Javey, *Proc. IEEE* **2019**, *107*, 2155; c) T. Ray, J. Choi, J. Reeder, S. P. Lee, A. J. Aranyosi, R. Ghaffari, J. A. Rogers, *Curr. Opin. Biomed. Eng.* **2019**, *9*, 47; d) H. C. Koydemir, A. Ozcan, *Annu. Rev. Anal. Chem.* **2018**, *11*, 127.

- [2] a) M. J. Tierney, J. A. Tamada, R. O. Potts, L. Jovanovic, S. Garg, C. R. Team, *Biosens. Bioelectron.* **2001**, *16*, 621; b) J. Heikenfeld, A. Jajack, J. Rogers, P. Gutruf, L. Tian, T. Pan, R. Li, M. Khine, J. Kim, J. Wang, J. Kim, *Lab Chip* **2018**, *18*, 217.
- [3] a) J. Heikenfeld, A. Jajack, B. Feldman, S. W. Granger, S. Gaitonde, G. Begtrup, B. A. Katchman, *Nat. Biotechnol.* **2019**, *37*, 407; b) J. Kim, A. S. Campbell, B. E. de Avila, J. Wang, *Nat. Biotechnol.* **2019**, *37*, 389; c) A. J. Bandothkar, W. J. Jeang, R. Ghaffari, J. A. Rogers, *Annu. Rev. Anal. Chem.* **2019**, *12*, 1; d) M. Mayer, A. J. Baeumner, *Chem. Rev.* **2019**, *119*, 7996; e) Q. Zhai, W. Cheng, *Mater. Today Nano* **2019**, *7*, 100041.
- [4] a) A. J. Bandothkar, W. J. Jeang, R. Ghaffari, J. A. Rogers, *Annu. Rev. Anal. Chem.* **2019**, *12*, 1; b) M. Bariya, H. Y. Y. Nyein, A. Javey, *Nat. Electron.* **2018**, *1*, 160; c) J. Choi, R. Ghaffari, L. B. Baker, J. A. Rogers, *Sci. Adv.* **2018**, *4*, eaar3921.
- [5] a) L. B. Baker, *Temperature* **2019**, *6*, 211; b) Z. Sonner, E. Wilder, J. Heikenfeld, G. Kasting, F. Beyette, D. Swaile, F. Sherman, J. Joyce, J. Hagen, N. Kelley-Loughnane, R. Naik, *Biomicrofluidics* **2015**, *9*, 031301.
- [6] M. J. Patterson, S. D. R. Galloway, M. A. Nimmo, *Exp. Physiol.* **2000**, *85*, 869.
- [7] H. Lee, T. K. Choi, Y. B. Lee, H. R. Cho, R. Ghaffari, L. Wang, H. J. Choi, T. D. Chung, N. S. Lu, T. Hyeon, S. H. Choi, D. H. Kim, *Nat. Nanotechnol.* **2016**, *11*, 566.
- [8] J. Choi, R. Ghaffari, L. B. Baker, J. A. Rogers, *Sci. Adv.* **2018**, *4*, eaar3921.
- [9] A. Koh, D. Kang, Y. Xue, S. Lee, R. M. Pielak, J. Kim, T. Hwang, S. Min, A. Banks, P. Bastien, M. C. Manco, L. Wang, K. R. Ammann, K. I. Jang, P. Won, S. Han, R. Ghaffari, U. Paik, M. J. Slepian, G. Balooch, Y. G. Huang, J. A. Rogers, *Sci. Transl. Med.* **2016**, *8*, 366ra165.
- [10] J. Choi, D. Kang, S. Han, S. B. Kim, J. A. Rogers, *Adv. Healthcare Mater.* **2017**, *6*, 1601355.
- [11] a) J. Choi, A. J. Bandothkar, J. T. Reeder, T. R. Ray, A. Turnquist, S. B. Kim, N. Nyberg, A. Hourlier-Fargette, J. B. Model, A. J. Aranyosi, S. Xu, R. Ghaffari, J. A. Rogers, *ACS Sens.* **2019**, *4*, 379; b) Y. Sekine, S. B. Kim, Y. Zhang, A. J. Bandothkar, S. Xu, J. Choi, M. Irie, T. R. Ray, P. Kohli, N. Kozai, T. Sugita, Y. X. Wu, K. Lee, K. T. Lee, R. Ghaffari, J. A. Rogers, *Lab Chip* **2018**, *18*, 2178.
- [12] a) J. Choi, Y. G. Xue, W. Xia, T. R. Ray, J. T. Reeder, A. J. Bandothkar, D. Kang, S. Xu, Y. G. Huang, J. A. Rogers, *Lab Chip* **2017**, *17*, 2572; b) S. B. Kim, Y. Zhang, S. M. Won, A. J. Bandothkar, Y. Sekine, Y. G. Xue, J. Koo, S. W. Harshman, J. A. Martin, J. M. Park, T. R. Ray, K. E. Crawford, K. T. Lee, J. Choi, R. L. Pitsch, C. C. Grigsby, A. J. Strang, Y. Y. Chen, S. Xu, J. Kim, A. Koh, J. S. Ha, Y. G. Huang, S. W. Kim, J. A. Rogers, *Small* **2018**, *14*, 1703334.
- [13] J. T. Reeder, J. Choi, Y. Xue, P. Gutruf, J. Hanson, M. Liu, T. Ray, A. J. Bandothkar, R. Avila, W. Xia, S. Krishnan, S. Xu, K. Barnes, M. Pahnke, R. Ghaffari, Y. Huang, J. A. Rogers, *Sci. Adv.* **2019**, *5*, eaau6356.
- [14] a) R. J. Maughan, S. M. Shirreffs, *Scand. J. Med. Sci. Sports* **2010**, *20*, 59; b) R. J. Maughan, S. M. Shirreffs, *Int. J. Sport Nutr. Exercise Metab.* **2008**, *18*, 457.
- [15] S. B. Kim, Y. Zhang, S. M. Won, A. J. Bandothkar, Y. Sekine, Y. Xue, J. Koo, S. W. Harshman, J. A. Martin, J. M. Park, T. R. Ray, K. E. Crawford, K. T. Lee, J. Choi, R. L. Pitsch, C. C. Grigsby, A. J. Strang, Y. Y. Chen, S. Xu, J. Kim, A. Koh, J. S. Ha, Y. Huang, S. W. Kim, J. A. Rogers, *Small* **2018**, *14*, 1703334.
- [16] A. S. Campbell, J. Kim, J. Wang, *Curr. Opin. Electrochem.* **2018**, *10*, 126.
- [17] a) W. Gao, S. Emaminejad, H. Y. Y. Nyein, S. Challa, K. V. Chen, A. Peck, H. M. Fahad, H. Ota, H. Shiraki, D. Kiriya, D. H. Lien, G. A. Brooks, R. W. Davis, A. Javey, *Nature* **2016**, *529*, 509; b) D. P. Rose, M. E. Ratterman, D. K. Griffin, L. L. Hou, N. Kelley-Loughnane, R. R. Naik, J. A. Hagen, I. Papautsky, J. C. Heikenfeld, *IEEE Trans. Biomed. Eng.* **2015**, *62*, 1457.
- [18] A. Hauke, P. Timmers, Y. R. Ojha, B. D. Cameron, R. Ballweg, T. Zhang, N. Twine, M. Brothers, E. Gomez, J. Heikenfeld, *Lab Chip* **2018**, *18*, 3750.
- [19] J. Kim, J. R. Sempionatto, S. Imani, M. C. Hartel, A. Barfidokht, G. Tang, A. S. Campbell, P. P. Mercier, J. Wang, *Adv. Sci.* **2018**, *5*, 1800880.
- [20] S. B. Kim, K. Lee, M. S. Raj, B. Lee, J. T. Reeder, J. Koo, A. Hourlier-Fargette, A. J. Bandothkar, S. M. Won, Y. Sekine, J. Choi, Y. Zhang, J. Yoon, B. H. Kim, Y. Yun, S. Lee, J. Shin, J. Kim, R. Ghaffari, J. A. Rogers, *Small* **2018**, *14*, 1802876.
- [21] H. Y. Y. Nyein, L. C. Tai, Q. P. Ngo, M. Chao, G. B. Zhang, W. Gao, M. Bariya, J. Bullock, H. Kim, H. M. Fahad, A. Javey, *ACS Sens.* **2018**, *3*, 944.
- [22] A. J. Bandothkar, P. Gutruf, J. Choi, K. Lee, Y. Sekine, J. T. Reeder, W. J. Jeang, A. J. Aranyosi, S. P. Lee, J. B. Model, R. Ghaffari, C. J. Su, J. P. Leshock, T. Ray, A. Verrillo, K. Thomas, V. Krishnamurthi, S. Han, J. Kim, S. Krishnan, T. Hang, J. A. Rogers, *Sci. Adv.* **2019**, *5*, eaav3294.
- [23] K. Wasserman, A. L. Van kesse, G. G. Burton, *J. Appl. Physiol.* **1967**, *22*, 71.
- [24] a) D.-H. Choi, Y. Li, G. R. Cutting, P. C. Searson, *Sens. Actuators, B* **2017**, *250*, 673; b) H. Xu, Y. F. Lu, J. X. Xiang, M. K. Zhang, Y. J. Zhao, Z. Y. Xie, Z. Z. Gu, *Nanoscale* **2018**, *10*, 2090.
- [25] L. J. Currano, F. C. Sage, M. Hagedon, L. Hamilton, J. Patrone, K. Gerasopoulos, *Sci. Rep.* **2018**, *8*, 15890.
- [26] a) H. Lee, C. Song, Y. S. Hong, M. S. Kim, H. R. Cho, T. Kang, K. Shin, S. H. Choi, T. Hyeon, D.-H. Kim, *Sci. Adv.* **2017**, *3*, e1601314; b) J. Kim, A. S. Campbell, J. Wang, *Talanta* **2018**, *177*, 163.
- [27] O. Parlak, S. T. Keene, A. Marais, V. F. Curto, A. Salleo, *Sci. Adv.* **2018**, *4*, eaar2904.
- [28] Z. Wen, Y. Yang, N. Sun, G. Li, Y. Liu, C. Chen, J. Shi, L. Xie, H. Jiang, D. Bao, *Adv. Funct. Mater.* **2018**, *28*, 1803684.
- [29] a) P. Maharjan, R. M. Toyabur, J. Y. Park, *Nano Energy* **2018**, *46*, 383; b) T. Sekine, R. Sugano, T. Tashiro, J. Sato, Y. Takeda, H. Matsui, D. Kumaki, F. D. Dos Santos, A. Miyabo, S. Tokito, *Sci. Rep.* **2018**, *8*, 4442.
- [30] a) K. Meng, J. Chen, X. Li, Y. Wu, W. Fan, Z. Zhou, Q. He, X. Wang, X. Fan, Y. Zhang, *Adv. Funct. Mater.* **2019**, *29*, 1806388; b) X. Fan, Y. Huang, X. Ding, N. Luo, C. Li, N. Zhao, S. C. Chen, *Adv. Funct. Mater.* **2018**, *28*, 1805045.
- [31] L. M. Tian, B. Zimmerman, A. Akhtar, K. J. Yu, M. Moore, J. Wu, R. J. Larsen, J. W. Lee, J. H. Li, Y. H. Liu, B. Metzger, S. B. Qu, X. G. Guo, K. E. Mathewson, J. A. Fan, J. Cornman, M. Fatina, Z. Q. Xie, Y. J. Ma, J. Zhang, Y. H. Zhang, F. Dolcos, M. Fabiani, G. Gratton, T. Bretl, L. J. Hargrove, P. V. Braun, Y. G. Huang, J. A. Rogers, *Nat. Biomed. Eng.* **2019**, *3*, 415.
- [32] a) S. R. Krishnan, T. R. Ray, A. B. Ayer, Y. J. Ma, P. Gutruf, K. Lee, J. Y. Lee, C. Wei, X. Feng, B. Ng, Z. A. Abecassis, N. Murthy, I. Stankiewicz, J. Freudman, J. Stillman, N. Kim, G. Young, C. Goudeseune, J. Cirraldo, M. Tate, Y. G. Huang, M. Potts, J. A. Rogers, *Sci. Transl. Med.* **2018**, *10*, eaat8437. b) S. Han, J. Kim, S. M. Won, Y. J. Ma, D. Kang, Z. Q. Xie, K. T. Lee, H. U. Chung, A. Banks, S. Min, S. Y. Heo, C. R. Davies, J. W. Lee, C. H. Lee, B. H. Kim, K. Li, Y. D. Zhou, C. Wei, X. Feng, Y. G. Huang, J. A. Rogers, *Sci. Transl. Med.* **2018**, *10*, eaan4950.
- [33] Y. J. Hong, H. Lee, J. Kim, M. Lee, H. J. Choi, T. Hyeon, D.-H. Kim, *Adv. Funct. Mater.* **2018**, *28*, 1805754.
- [34] S. Nakata, T. Arie, S. Akita, K. Takei, *ACS Sens.* **2017**, *2*, 443.
- [35] a) D. P. Rose, M. Ratterman, D. K. Griffin, L. Hou, N. Kelley-Loughnane, R. K. Naik, J. A. Hagen, I. Papautsky, J. Heikenfeld, Proceedings of the 36th Annu. Int. Conf. IEEE Engineering in Medicine and Biology Society, IEEE, Chicago, IL,

- USA 2014; b) H. Y. Y. Nyein, M. Bariya, L. Kivimaki, S. Uusitalo, T. S. Liaw, E. Jansson, C. H. Ahn, J. A. Hangasky, J. Q. Zhao, Y. J. Lin, T. Happonen, M. H. Chao, C. Liedert, Y. B. Zhao, L. C. Tai, J. Hiltunen, A. Javey, *Sci. Adv.* **2019**, *5*, eaaw9906.
- [36] MC10 Receives FDA 510(k) Clearance for the BioStamp nPoint™ System, <https://www.mc10inc.com/press-media/fda-510k-clearance-for-the-biostamp-npoint-system> (accessed: October 2019).
- [37] How wearable sweat trackers are providing athletes with critical hydration insights, <https://www.wearable.com/features/gatorade-gx-sweat-patch-vision-7222> (accessed: October 2019).
- [38] L'Oréal Unveils Prototype Of First-Ever Wearable Microfluidic Sensor To Measure Skin pH Levels, <https://www.prnewswire.com/news-releases/loreal-unveils-prototype-of-first-ever-wearable-microfluidic-sensor-to-measure-skin-ph-levels-300773342.html> (accessed: October 2019).